ACS APPLIED MATERIALS & INTERFACES

www.acsami.org

Research Article

Advanced Drug Delivery Modulation via Hybrid Nanofibers Enhances Stem Cell Differentiation

Jeffrey Luo, Letao Yang, Sy-Tsong Dean Chueng, Brian Conley, Christopher Rathnam, and Ki-Bum Lee*

Cite This: *ACS Appl. Mater. Interfaces* 2022, 14, 34488−34501

Read Online

ACCESS | Metrics & More | Article Recommendations | Supporting Information

ABSTRACT: Seamlessly integrating soluble factors onto biomedical scaffolds with a precisely manufactured topography for efficient cell control remains elusive since many scaffold fabrication techniques degrade payloads. Surface adsorption of payloads onto synthesized nanoscaffolds retains bioactivity by removing exposure to harsh processing conditions at the expense of inefficient drug loading and uncontrolled release. Herein, we present a nanomaterial composite scaffold paradigm to improve physicochemical surface adsorption pharmacokinetics. As a proof of concept, we integrated graphene oxide (GO) and manganese dioxide (MnO_2) nanosheets onto nanofibers to increase loading capacity and tune drug release. Non-degradable GO enhances payload retention, while biodegradable MnO_2 enables cell-responsive drug release. To demonstrate the utility of this hybrid nanomaterial scaffold paradigm for tissue engineering, we adsorbed payloads ranging from small molecules to proteins onto the scaffold to induce myogenesis and osteogenesis for multiple stem cell lines. Scaffolds with adsorbed payloads enabled more efficient differentiation than media supplementation using equivalent quantities of differentiation factors. We attribute this increased efficacy to a reverse uptake mechanism whereby payloads are localized around seeded cells, increasing delivery efficiency for guiding differentiation. Additionally, we demonstrate spatial control over cells since differentiation factors are delivered locally through the scaffold. When co-culturing scaffolds with and without adsorbed payloads, only cells seeded on payload-adsorbed scaffolds underwent differentiation. With this modular technology being capable of enhancing multiple differentiation fates for specific cell lines, this technology provides a promising alternative for current tissue engineering scaffolds.

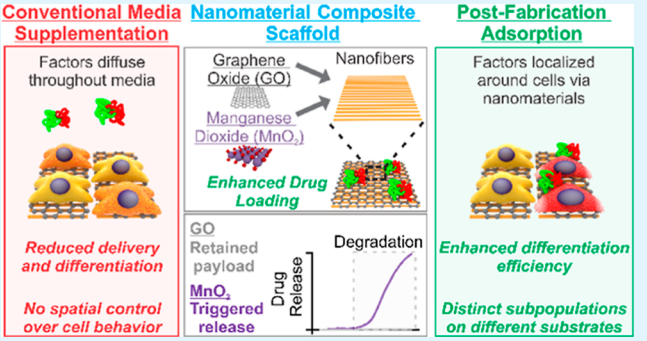

KEYWORDS: *nanoscaffolds, advanced drug delivery, hybrid nanomaterials, stem cell differentiation, tissue engineering*

1. INTRODUCTION

Musculoskeletal wounds represent some of the most commonplace injuries requiring medical attention.[1,2] Sources vary from injuries such as vehicular trauma to genetically linked disorders such as osteoarthritis. Such injuries can result in decreased mobility, diminished quality of life, tissue morbidity, and long-term financial burden. In the event pharmaceuticals and surgical techniques prove ineffective at treating musculoskeletal injuries (e.g., critical size defects), tissue engineering interventions may be necessary to rescue and repair severely affected areas. To bolster the efficacy of tissue engineering approaches, stem cell-based therapies can be employed to replace and regenerate the damaged musculoskeletal tissue (Figure 1a).[1−3] The ability to generate *de novo* myocytes and osteoblasts is of particular importance since muscles rely on cellular activity to generate contractile forces and osteoblasts constantly assist in remodeling bones.[1−3] Mesenchymal stem cells offer an attractive source of replacement cells when a significant injury deprives the local area of resident cells.

A critical barrier for implementing stem cell therapies in the clinic is ensuring control over cellular behavior after transplantation. The most common method is to seed cells onto scaffolds that are pre-designed with various behavior control stimuli ranging from peptides and small molecule payloads to precisely tuned biomechanical substrate characteristics. To maximize the efficacy of payload-based approaches, high drug loading is favorable since in vivo environments can decrease bioactivity via clearance and degradation.

Attempts to integrate exogenous stem cell control stimuli onto scaffolds have often been hampered by harsh processing conditions (e.g., organic solvents, shear forces, and heating) inherited from many scaffold fabrication systems.[1,3−5] For sensitive payloads such as proteins and peptides, direct incorporation into the pre-processed scaffold precursors may prove problematic as many scaffold fabrication techniques can

Received: June 9, 2022
Accepted: July 11, 2022
Published: July 21, 2022

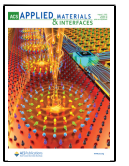

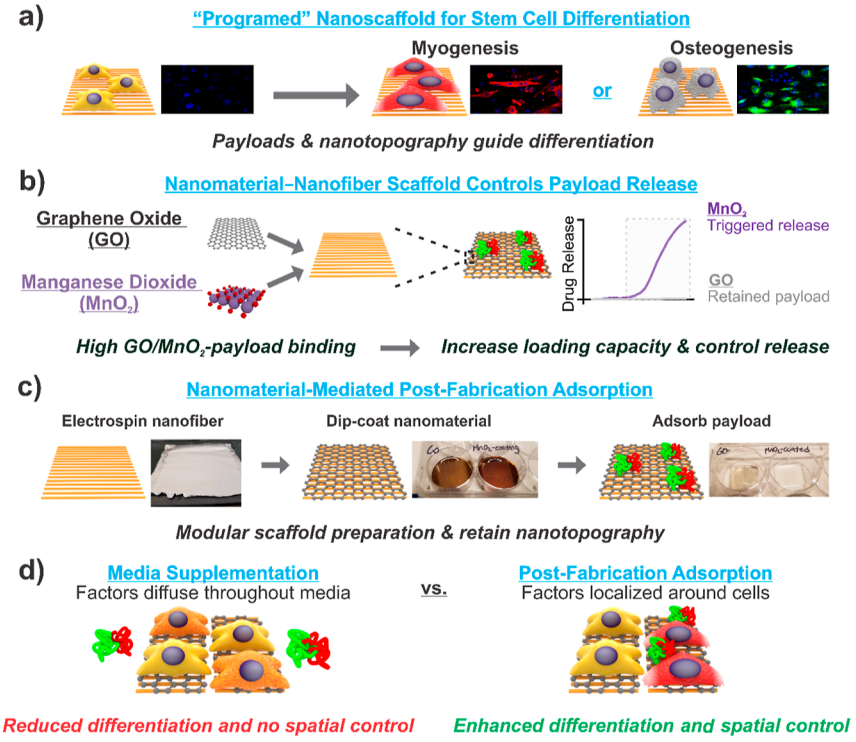

Figure 1. Scheme for the design of hybrid nanomaterial–nanofiber composite scaffolds. (a) In an ideal musculoskeletal tissue engineering therapy, stem cells are taken from a patient, seeded onto a scaffold (e.g., nanofibers) with cell behavior cues (e.g., differentiation factors), and transplanted back into the injury site to assist in the regeneration of muscle and bone tissue. (b) To improve tissue engineering therapies, we integrated GO and manganese dioxide (MnO_2) to form composite scaffolds that feature increased drug binding affinity (to increase loading capacity) and well-defined biodegradation behavior (to control release). GO does not readily degrade, nor releases payloads, while MnO_2 releases adsorbed payloads when exposed to bioreductants. Moreover, large quantities of differentiation factors can be adsorbed directly onto biomedical scaffolds, which improves delivery to seeded stem cells and differentiation efficiency. (c) These composite scaffolds can be readily prepared by dip-coating nanofibers in nanomaterial solutions, followed by drop-casting the payload solution for nanomaterial-mediated post-fabrication adsorption. (d) While conventional medium supplementation suffers from reduced delivery, low differentiation efficiency, and no spatial control due to diffusion, our work in adsorbing differentiation factors onto nanomaterial-coated nanofibers localizes the differentiation factors nearby the seeded cells to significantly enhance stem cell differentiation and spatial control.

cause protein denaturation and loss of bioactivity. Post-fabrication modification is an alternative whereby the scaffold is fabricated before the payload is integrated.[4,5] While several post-fabrication loading techniques have been developed, such as covalent immobilization and host–guest interactions, chemical modification of the drug molecules is often required, leading to compromised biological activity. Physical adsorption (e.g., dip-coating and drop-casting) relies on weak, non-specific interactions to load payloads onto fabricated scaffolds, resulting in better-preserved bioactivity. Despite these benefits, conventional physical adsorption systems such as highly porous scaffolds and current surface modifications still suffer from uncontrolled burst release kinetics.[6]

This key deficiency in physical adsorption can be improved by forming composite scaffolds capable of more robust physicochemical interactions. These physicochemical interactions (e.g., $\pi-\pi$, hydrogen bonding, van der Waals, and electrostatic) exhibit higher binding energies than simple physical interactions (e.g., van der Waals), which mitigates premature burst release and increases loading capacity.[7,8] Specifically, nanomaterials are uniquely suited for augmenting surface-based physicochemical adsorption due to a high surface-area-to-volume ratio, a wide variety of physicochemical interactions, and high protein binding energies.[7−10] Moreover, small quantities of nanomaterials are needed to enact significant changes in surface chemistry, allowing bulk scaffold properties to remain relatively unchanged. The prior literature attests to nanomaterial surface coatings for various practical applications such as drug delivery, modulating surface stiffness, and adsorbing environmental analytes. In this report, we employ nanomaterials to form modular composite scaffolds to advance the field of tissue engineering.

As a proof of concept, graphene oxide (GO) and manganese dioxide (MnO_2) nanosheets were selected to generate hybrid nanomaterial composite scaffolds. As one of the most explored nanomaterials, GO has been investigated for various biomedical applications, including increasing electrical conductivity of nerve conduits, augmenting mechanical stiffness of bone-regenerative scaffolds, and modulating drug pharmacokinetics.[9−11] Conversely, MnO_2 has seen recent interest for its ability to undergo redox reactions in vivo to release MRI-active byproducts and ameliorate oxidative stresses.[6,12−14] In addition, these two nanomaterials were selected due to previous demonstrations of high binding affinity to common biological functional groups, high protein loading capacity imparted from various nonspecific interactions (e.g., $\pi-\pi$, hydrogen bonding, van der Waals, and electrostatic), and low rates of adsorption-induced denaturation (Figure 1b).[6,9−13,15−19]

The crucial parameter that distinguishes MnO_2 from GO within the context and application of this work is biodegradability. MnO_2 is readily degraded with bioreductants

https://doi.org/10.1021/acsami.2c10288
ACS Appl. Mater. Interfaces 2022, 14, 34488−34501

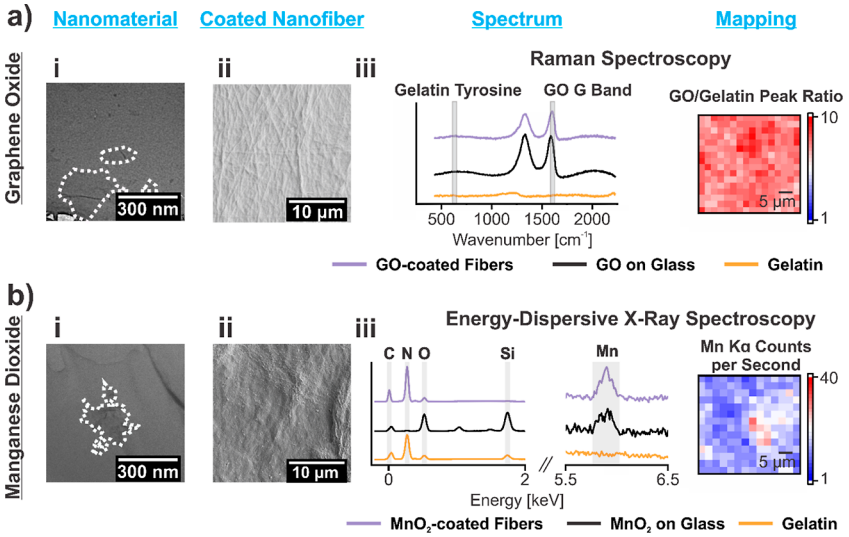

Figure 2. Characterization of hybrid nanomaterial−nanofiber composite scaffolds. (a,b-i) Representative TEM images showing the successful synthesis of monolayer GO (a) and MnO_2 (b) nanosheets. (a,b-ii) Representative FE-SEM images showing complete nanomaterial adsorption over nanofibers. Nanofiber morphology is still visible under nanomaterials. (a,b-iii) Raman and EDS spectra for gelatin nanofibers, nanomaterials drop-casted on glass, and hybrid nanomaterial−nanofiber composites confirm successful adsorption. Specifically, GO-coated nanofibers show characteristic GO-G Raman peaks, and MnO_2-coated nanofibers show characteristic manganese Kα EDS peaks. Raman spectroscopy and EDS mapping over a 30 × 30 μm area show homogeneous nanomaterial adsorption as per the relatively low variation in the GO-G/gelatin−tyrosine Raman peak ratio and manganese Kα EDS peak, respectively.

such as glutathione, while GO shows negligible degradation in most biological systems (Figure 1b).[6,10,12,13] This confers a substantial advantage to nanomaterial-mediated adsorption as conventional porous scaffolds lack precise release tunability.[6] This critical difference can significantly alter the bioactivity of adsorbed differentiation factors since degradation-mediated release may be favorable for some payloads (e.g., targets for intracellular receptors) while irreversible binding may be preferred for others (e.g., targets for cell surface receptors).[20]

For this demonstration, gelatin nanofibers were selected as the biomedical scaffold due to (1) gelatin biodegradability, biocompatibility, and molecular similarity to collagen, (2) aligned nanotopography capable of activating biomechanical pathways supporting stem cell differentiation, and (3) the electrospinning fabrication technique that readily translates to commercial-scale manufacturing.[5,21,22] Human clinical trials using gelatin-based scaffolds attest to the regulatory appeal and clinical potential of this biomaterial.[21] Moreover, electrospinning nanofibers result in the degradation of sensitive protein payloads, which presents a clear motivation and need to improve physicochemical adsorption for biomedical applications.[4,5]

Herein, we realize a nanomaterial composite scaffold paradigm with (1) modulated payload pharmacokinetics, (2) biophysical cues from the underlying nanotopography, and (3) tunable biodegradability that can be "programed" to enhance a specific differentiation lineage by adsorbing specific payloads. This unique combination of features provides significant control over drug release. Since the composite scaffold preparation is highly modular, we can select various differentiation factor payloads (e.g., small molecules to large multisubunit proteins) independently from nanomaterials without reoptimizing adsorption protocols (Figure 1c). Moreover, localizing differentiation factors to the composite scaffold enhances differentiation efficiency compared to conventionally dissolved factors and enables co-culture systems with multiple cell types derived from a single parent cell population (Figure 1b,d). Since this technique can be readily extended to include other emerging nanomaterials and novel payloads, we envision this platform technology to be applied to generate stem cell regenerative therapies with increased control over cell behaviors and off-target payload effects across a wide variety of scaffold architectures and target tissues.

2. RESULTS AND DISCUSSION

2.1. Preparation and Characterization of Hybrid Nanomaterial−Nanofiber Scaffolds. Nanofibers are one of the most common tissue engineering scaffolds due to their similarities with structural proteins (e.g., collagen) that form nano-scale fiber assemblies.[1,2,4,5,22] To form nanofiber scaffolds, we used electrospinning because of its compatibility with various polymers, tunable processing parameters, and process scalability.[4,5,22] Since it has been demonstrated that collagen assembles into 200 nm fibrils to support cell growth, we optimized electrospinning parameters to create 100−200 nm nanofibers, as verified by field-emission scanning electron microscopy (FE-SEM) (Figure S1).[23,24] A rotating mandrel was used to align the nanofibers, which has been shown to increase the differentiation of stem cells in the Supporting Information (Figure S1) along with various other reports.[25,26] After electrospinning, fibers were crosslinked to allow aqueous stability during nanomaterial adsorption and cell applications. These electrospun gelatin nanofibers provide a base for our platform with an ideal surface nanotopography for controlling the cell fate.

To address key deficiencies in physical adsorption related to loading capacity and uncontrolled release, we explored using GO and manganese dioxide (MnO_2). GO and MnO_2 nanosheets are (tri-)atomically thin nanomaterials that (1) are ideal surface coatings to maintain the underlying fiber topography and (2) exhibit high binding affinity for biomolecules and drugs due to their unique physicochemical

https://doi.org/10.1021/acsami.2c10288
ACS Appl. Mater. Interfaces 2022, 14, 34488−34501

properties.[6,10−13] Moreover, protein adsorption and release on GO- and MnO_2-coated surfaces have been demonstrated to induce negligible denaturation in the prior literature.[18,19] After synthesizing GO and MnO_2 nanosheets, X-ray photoelectron spectroscopy (XPS) confirmed the appropriate elemental composition and chemical states for both nanomaterials (Figure S2a,b). Transmission electron microscopy (TEM, Figure 2a,b-i) and atomic force microscopy (AFM) (Figure S3) indicated that GO and MnO_2 were mostly single-layer nanosheets (∼1−2 nm) with sparse multilayered aggregates (<10 layers), while dynamic light scattering (Figure S2c) showed 50−100 nm lateral dimensions for MnO_2 and 100−300 nm for GO. Both products exhibit strong negative zeta potentials (Figure S2d) and are colloidally stable in water for more than 1 month.

The homogeneity of nanomaterial coatings was visualized using FE-SEM (Figures 2a,b-ii and S4) and characterized using Raman spectroscopy and electron-dispersive X-ray spectroscopy (Figure 2a,b-iii) over a large area. GO tends to form a sheet over the nanofibers (i.e., fewer discontinuities between nearby fibers), while MnO_2 appears to be wrapped around individual nanofibers (Figure S4). Though the FE-SEM images suggest a moderate loss of nanofiber topography cues (i.e., reverted to the 2D sheet scaffold), C2C12 cells seeded on aligned nanofibers experienced enhanced myogenesis compared to unaligned nanofibers (Figure S1). Since aligned nanofibers are known to enhance myogenesis, we conclude that nanofiber topography and alignment were preserved even after nanomaterial adsorption.[25,26] As a rough measure of hydrophilicity, an important feature for cell attachment, contact angle measurements revealed that neither nanomaterial resulted in substantial changes (Figure S5).[27,28]

Our hybrid nanomaterial−nanofiber scaffold can be routinely prepared with robust GO and MnO_2 coatings on our gelatin nanofibers. Moreover, the facile and modular nature of nanomaterial dip-coating can be extended to emergent nanomaterials and biomedical scaffolds, broadening the applicability of this nanomaterial composite scaffold paradigm.

2.2. Fluorescein Isothiocyanate-Labeled Payload Adsorption on Hybrid Scaffolds. After adsorbing the two nanomaterials onto the nanofiber scaffolds, drug adsorption and loading capacity were investigated. A series of model proteins [bovine serum albumin (BSA), gelatin, and lysozyme] and differentiation factors [insulin and transferrin (IT)] were labeled with fluorescein isothiocyanate (FITC) (Figure 3a). GO- and MnO_2-coated nanofibers were saturated with (1) 15.5 μg mL^{-1} FITC model protein or (2) a mixture of 10 μg mL^{-1} insulin and 5.5 μg mL^{-1} transferrin to mimic differentiation factor-loaded scaffold preparation. These values mimic the concentration of commercially available IT mixtures recommended for myogenesis (e.g., insulin−transferrin−selenium, Gibco). Once adsorbed, the substrates were washed to remove weakly adsorbed (e.g., multilayered) proteins before assessing the loading capacity (Figure S6).

Most proteins showed greater adsorption on GO- and MnO_2-coated nanofibers than on bare nanofibers (Figure 3a). This noticeable increase in loading capacity is attributed to the wide variety of high-binding-energy, nonspecific interactions (e.g., $\pi-\pi$, hydrogen bonding, van der Waals, and electrostatic) between GO and MnO_2 with their protein payloads.[10,12] One notable exception is gelatin, commonly used as a coating material for tissue culture plastic. With the significantly higher loading capacity of our composite scaffolds, we can deliver a greater quantity of bioactive payloads to target cells for greater stem cell differentiation efficiency.

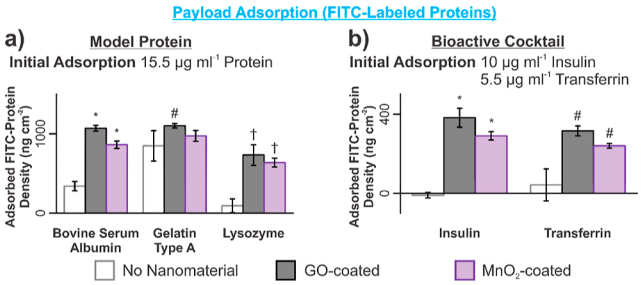

Figure 3. Enhanced protein payload adsorption on nanomaterial−nanofiber composites. Both GO- and MnO_2-coated nanofibers enhance loading capacity for FITC-labeled model protein solutions (a) and myogenic differentiation factor cocktails (b). One-way ANOVA followed by Dunnett's test for each FITC−protein group (α = 0.05, the symbol indicates a statistically significant difference against bare nanofibers, n = 3). One exception is gelatin, a denatured collagen derivative commonly used to coat tissue culture plastic.

An interesting finding is the density of protein adsorbed onto composite scaffolds. Since payload adsorption is expected to be a surface phenomenon, we can anticipate proteins to form a monolayer on the substrates after washing to remove excess weakly adsorbed proteins.[29,30] This due to the monolayer preventing robust interactions between additional payload molecules and the underlying substrate. Previous literature studies using BSA report monolayer densities between 100 and 500 ng cm^{-1}, whereas loading capacities for GO- and MnO_2-coated nanofibers exceed this figure.[29,30] We attribute this increase in loading capacity to a high surface area from the multilayer, porous nanofiber mat. The densities reported in Figure 3a use the nominal, macroscopic surface area of the nanomaterial−nanofiber composite scaffolds, which underestimates the actual surface area that is available for payload adsorption. For regenerative therapies, the roughness of the nanofiber scaffold (with or without nanomaterials) is advantageous since it augments drug loading capacity.

2.3. Characterization of Payload Release. For payloads acting on intracellular receptors, release from the substrate for cellular uptake in a degradation-mediated manner allows for enhanced control of stem cell differentiation.[20] Conversely, several differentiation factors acting upon cell surface receptors become more bioactive when irreversibly bound onto scaffolds.[31,32] Maximizing the utility of the nanomaterial composite scaffold paradigm requires investigation into both degradable and non-degradable nanomaterials that allow for either payload release or retention. To investigate the release profile of our hybrid nanomaterial−nanofiber scaffold, we employed surface plasmon resonance (SPR) and the enzyme-linked immunosorbent assay (ELISA) to monitor short-term and long-term drug release, respectively.

2.3.1. SPR Real-Time Characterization of Short-Term Payload Release. While GO is slow to degrade, MnO_2 can rapidly degrade under reducing conditions, making them an ideal pair for studying modular biodegradability to control drug release.[6,12,13] To confirm the tunability of drug release, we utilized SPR to monitor the adsorbed mass on a uniform, nanomaterial-coated surface. Both negatively charged nanomaterials (Figure S2d) form electrostatic interactions with the positively charged SPR sensors, leading to stable coatings that

https://doi.org/10.1021/acsami.2c10288
ACS Appl. Mater. Interfaces 2022, 14, 34488−34501

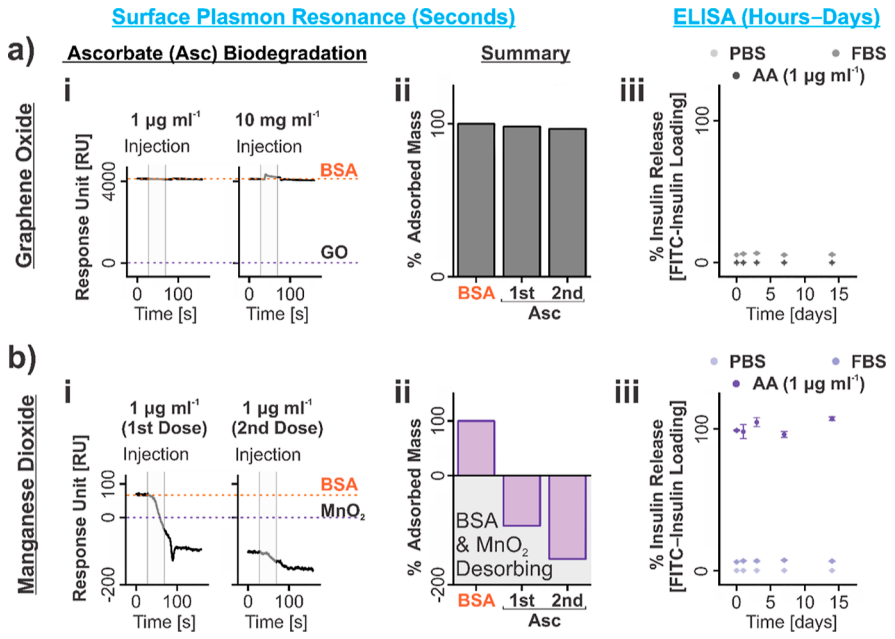

Figure 4. Tunable release behavior on nanomaterial−nanofiber composites. Payload release was characterized via SPR (short-term) and the ELISA (long-term). To examine short-term drug release, BSA was adsorbed onto GO- and MnO_2-coated SPR chips. These protein-adsorbed chips were subsequently subjected to ascorbic acid solutions to examine biodegradation (a,b-i). Adsorbed BSA mass undergoes negligible release on GO-coated sensors due to negligible biodegradation, while MnO_2-coated sensors experience a significant decrease in adsorbed mass attributed to both releases of BSA and degradation of underlying MnO_2 (a,b-ii). (a,b-iii) To examine long-term drug release, insulin was adsorbed onto GO- and MnO_2-coated gelatin nanofiber substrates and incubated in either (1) PBS, (2) FBS, or (3) ascorbic acid (1 μg mL^{-1}, AA) in PBS. PBS failed to induce significant insulin release over the 14 day test period, while FBS incubation resulted in ∼5% release (e.g., Vroman effect). The greatest difference was observed with AA, whereby GO-coated substrates released negligible quantities of insulin while MnO_2-coated substrates released nearly all adsorbed insulin within the 1st hour.

resist solution flow. Once the nanomaterial solutions were adsorbed and stabilized on the activated amine-functionalized chips, a new baseline value was taken (Figure S7a,b-i), and BSA solution was introduced into the flow cell (Figure S7a,b-ii). Positive RU values after BSA injection indicate that (1) the BSA successfully adsorbed onto nanomaterial-coated sensors and (2) nanomaterial sensor immobilization remains stable during solution flow.

An unexpected result is the lower BSA loading capacity on MnO_2 than on GO. This discrepancy is attributed to limitations with amine-functionalized SPR chips. These chips are activated by acidic solutions to protonate amine groups for adequate electrostatic attraction and ligand/nanomaterial loading; however, low pH solutions induce MnO_2 aggregation within the SPR flow cell (Figure S8). The SPR results shown here are the product of compromising low acid concentration for enhanced MnO_2 stability with an adequately low pH to activate amine groups for electrostatic loading. Conversely, GO exhibits high stability across a wider range of pH values. These nanomaterial SPR sensor limitations do not exist for nanomaterial−nanofiber composite scaffold preparation since other interactions (e.g., $\pi-\pi$, hydrogen bonding, van der Waals, and electrostatic) can stabilize nanomaterial−gelatin and nanomaterial−payload interactions at the physiological, neutral pH.[10,13,15−17]

To characterize biodegradability, ascorbic acid was used as a bioreductant to induce the release of adsorbed BSA (Figure 4a,b-i). Even at supraphysiological concentrations of ascorbic acid (10 mg mL^{-1}), GO-coated chips released negligible quantities of BSA (Figure 4a-ii). This contrasts with MnO_2-coated chips, which exhibited complete release of BSA and even degradation of MnO_2 (as evidenced by the negative RU signal) at physiological concentrations of ascorbic acid (1 μg mL^{-1}) (Figure 4b-ii).[33] As the MnO_2 coating degrades, nanomaterial−payload interactions (e.g., $\pi-\pi$, hydrogen bonding, van der Waals, and electrostatic) are lost, which releases the payload into the media. This release does not occur with GO-coated substrates since nanomaterial−payload interactions remain intact due to the extraordinary stability of GO. In fact, a portion of BSA on GO-functionalized chips proved resistant to sequential application of various dissociation buffers (i.e., acidic, alkaline, hydrophobic, chaotropic, and ionic buffers in supraphysiological concentrations) (Figure S9).[34] Rapid biodegradation of MnO_2 is intrinsically linked to the rapid release of the BSA payload. Meanwhile, non-degrading GO does not release the model drug under physiological conditions.

Here, we demonstrated the strategic selection of nanomaterials that can impart significant control over short-term (seconds to minutes) drug release profiles by modulating surface coating degradation. Although physical adsorption of drugs onto conventional porous scaffolds (e.g., nanofibers) is associated with uncontrolled burst release, we present two alternative modes for control over adsorbed payloads. Within the context of musculoskeletal regeneration and tissue engineering, MnO_2 coatings are recommended when targeting intracellular receptors since payloads are released and made available for uptake upon nanomaterial degradation.[20] In contrast, GO coatings are more suited to robustly bind payloads onto the scaffold for cell surface receptors when nanomaterial degradation and payload release is undesirable.[31,32]

https://doi.org/10.1021/acsami.2c10288
ACS Appl. Mater. Interfaces 2022, 14, 34488−34501

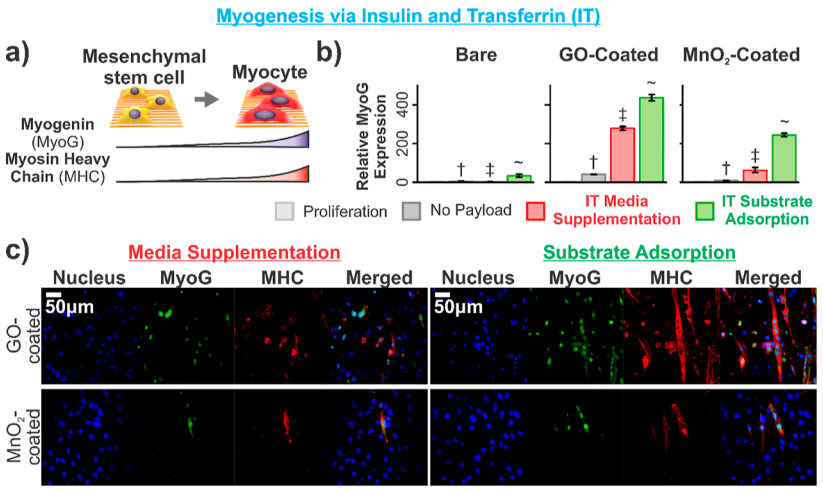

Figure 5. C2C12 myogenesis is enhanced on nanomaterial−nanofiber composite substrates with adsorbed differentiation factors. (a) Schematic diagram illustrating expression patterns for myogenesis. As cells undergo myogenesis to form myocytes, Myogenin and MHC expressions increase. (b) Myogenesis characterization via RT-qPCR reveals that C2C12 cultured on nanomaterial−nanofiber composite scaffolds with adsorbed myogenesis factors IT expressed greater quantities of MyoG and MHC compared to samples where an equivalent mass of adsorbed IT was administered as a media supplement. (c) Additionally, GO-coated scaffolds with adsorbed IT were able to induce cell fusion and generate multinucleated cells. MnO_2-coated substrates showed negligible cell fusion and lower MyoG and MHC expression than GO-coated substrates, potentially due to detrimental effects of MnO_2 biodegradation products (i.e., Mn^{2+}) reported elsewhere for myogenesis. Additional controls involving non-myogenic payloads and media supplements in excess substrate loading capacities are reported in Figure S11. RT-qPCR was analyzed using one-way ANOVA, followed by Tukey's HSD within each nanomaterial group [$\alpha = 0.05$, * indicates a statistically significant difference; †, ‡, and ∼ indicate a statistically significant difference against all other conditions with different symbols, analysis for myogenesis was performed with additional controls shown in Figure S11, $n = 3$].

2.3.2. ELISA Characterization of Long-Term Payload Release in Physiological Media. While SPR is useful for real-time analysis of binding and release phenomena, several limitations necessitate complementary drug release characterization to better understand payload desorption in physiological conditions (e.g., in the presence of serum). Most notably, SPR cannot differentiate background signals from serum proteins adsorbing onto the sensor chip. The ELISA is ideal to measure drug release in serum-containing media due to the high analyte specificity and low background interference from serum proteins. Thus, the human insulin ELISA was employed to measure the release of insulin from GO- and MnO_2-coated nanofibers in three different media: phosphate-buffered saline (PBS), fetal bovine serum (FBS), and ascorbic acid (1 $\mu g\ mL^{-1}$) in PBS.

Prolonged incubation (14 days) of insulin-adsorbed GO- and MnO_2-coated nanofibers in PBS failed to release significant quantities of insulin (<5% of FITC−insulin loading capacity) (Figure 4a,b-iii). This inability to release adsorbed insulin is likely due to various nonspecific interactions (e.g., $\pi-\pi$, hydrogen bonding, van der Waals, and electrostatic) between GO/MnO_2 and insulin.[10,12] The high binding energy from these interactions limits insulin release over a time scale appropriate for stem cell differentiation and tissue engineering applications. Conversely, incubation with ascorbic acid yielded different drug release profiles in GO- and MnO_2-coated nanofibers (Figure 4a,b-iii). GO-coated nanofibers failed to release significant quantities of insulin over the 14 day test period, while MnO_2-coated nanofibers underwent near-complete insulin release within the 1st hour. This is expected as SPR revealed complete MnO_2 biodegradation and BSA release within minutes of ascorbic acid introduction.

Incubation in FBS produced some insulin release (∼5 to 10% for both nanomaterials) (Figure 4a,b-iii). This non-specific, competitive serum protein adsorption/desorption behavior on surfaces (i.e., Vroman effect) is well-characterized in the literature.[35−37] The ability for serum proteins to nonspecifically replace the adsorbed insulin is minimized due to adsorption of the insulin payload prior to serum protein exposure and high binding energy.[35−37]

These drug release results demonstrate the utility of GO and MnO_2 to control drug release from hybrid nanomaterial−nanofiber scaffolds. Both nanomaterials exhibit high binding energy due to nonspecific interactions with proteins, which limit payload desorption and release even in physiological media (e.g., serum).

2.4. Modular Enhanced Stem Cell Differentiation on Payload-Adsorbed Hybrid Scaffolds. Stem cell therapy is hampered by imprecise differentiation control. Incorporation of soluble factors (e.g., insulin) and physical signaling (e.g., nanofiber topography) cues into a single scaffold remains a significant problem.[9] Our nanomaterial−nanofiber scaffold provides the unique ability to independently modulate both cues without compromising either modality. Moreover, the hybrid scaffold's enhanced loading capacity and modular drug release provide superior payload delivery compared to conventional nanofibers. For an initial demonstration, C2C12 were used for their (1) ability to differentiate into myocytes and osteoblasts and (2) established role in the musculoskeletal literature after verifying GO and MnO_2 to be nontoxic (Figure S10).[38]

2.4.1. Induction of Myogenesis in C2C12. To induce C2C12 myogenesis, IT were chosen as differentiation factors due to established use in the literature (Figure 5a).[39] Myogenesis was quantified via the reverse transcriptase quantitative polymerase chain reaction (RT-qPCR) and immunocytochemistry (ICC) staining for myogenin (MyoG) and myosin heavy chain (MHC) (Figure 5a).[40] The potency of differentiation factors adsorbed onto the composite scaffold ("IT Substrate Adsorption") was tested against the same

https://doi.org/10.1021/acsami.2c10288
ACS Appl. Mater. Interfaces 2022, 14, 34488−34501

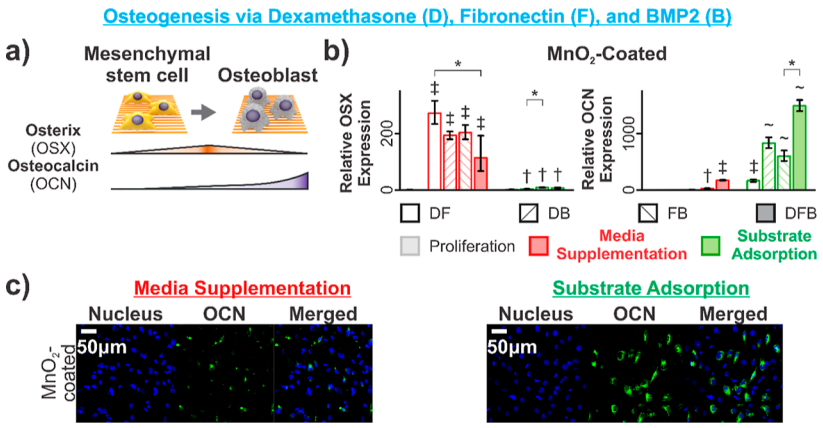

Figure 6. C2C12 osteogenesis is enhanced on nanomaterial−nanofiber composite substrates with adsorbed differentiation factors. (a) Schematic diagram illustrating expression patterns for osteogenesis. Cells undergoing osteogenesis express high levels of OSX as intermediate pre-osteoblasts. This decreases as cells progress to terminally differentiated osteoblasts, which express OCN. (b) Since DEX was found to exert a negligible effect on osteogenesis when adsorbed onto GO-coated nanofibers (Figure S12), only MnO_2-coated nanofibers were used in the following osteogenesis experiments. Osteogenesis characterization via RT-qPCR reveals that C2C12 cultured on nanomaterial−nanofiber composite scaffolds with various combinations of adsorbed DEX, fibronectin, and bone morphogenetic protein-2 (DFB) upregulated OCN and downregulated OSX compared to cells cultured with DFB administered as media supplements. Additionally, the adsorption of numerous heterogeneous differentiation factors (i.e., small molecules, soluble peptides, and ECM proteins) was demonstrated to cooperate and further enhance osteogenesis. (c) These results were mirrored in ICC as substrate adsorption resulted in greater immunofluorescence staining for OCN. RT-qPCR was analyzed using one-way ANOVA, followed by Tukey's HSD within each nanomaterial group [$\alpha = 0.05$; †, ‡, and ∼ indicate a statistically significant difference against all other conditions with different symbols; * indicates a statistically significant difference; $n = 3$ biological replicates].

quantity of differentiation factors supplemented to the media ("IT Media Supplementation"), as determined in Figure 3b. Scaffolds without any administered payload ("No Payload") were included alongside a proliferation control on tissue culture plastic.

While bare GO- and MnO_2-coated nanofibers induced myogenesis, the effects were negligible. IT substrate adsorption on both GO- and MnO_2-coated scaffolds resulted in greater enhancement of MyoG expression compared to simple media supplementation (Figure 5b). This enhancement correlated with an increase in MyoG and MHC in ICC staining for "Substrate Adsorption" compared to "Media Supplementation" (Figure 5c). An additional control, non-myogenic, adsorbed payload BSA ("BSA Substrate Adsorption") was included to verify that results from IT adsorption are due to targeted action on key myogenesis pathways (Figure S11).

The mechanism of enhanced differentiation is likely similar to the previously reported reverse uptake.[41] Differentiation factors supplemented in media become dispersed due to diffusion. Individual molecules may not reach the target cell before degradation or sequestration. Differentiation factor adsorption localizes the payloads onto the substrate that cells adhere to, thus increasing the delivery and differentiation efficiency. Nanomaterial composite scaffolds improve upon the reverse uptake mechanism by increasing the loading capacity and controlling release of differentiation factors, further bolstering stem cell differentiation compared to bare scaffolds.

While substrate adsorption significantly increases payload biopotency (i.e., capacity for a given mass of material to elicit a biological response), the nanomaterial hybrid scaffold is limited by the available surface area for payload adsorption. This limitation is seen when comparing "IT Substrate Adsorption" to the literature-recommended "Excess IT Media Supplementation" that exceeds substrate loading capacity (Figure S11). While "IT Substrate Adsorption" achieved roughly 50% of the MyoG expression seen in "Excess IT in Media Supplementation", approximately 20% of the supplemented IT was required to achieve these results when adsorbed onto the scaffold. The demonstrated increase in biopotency is advantageous as differentiation factors can elicit significant side effects when used in excessive quantities.

2.4.2. Induction of Osteogenesis in C2C12. Numerous stem cells can undergo differentiation into several cell fates, which is advantageous for tissue engineering since heterogeneous tissues need to be generated from a single parent stem cell line. C2C12 can undergo myogenesis and osteogenesis, so we demonstrate the modularity of this nanomaterial composite paradigm to target multiple differentiation pathways.[38] Two markers were used to discern intermediate pre-osteoblasts (osterix, OSX) from terminally differentiated osteoblasts (osteocalcin, OCN) (Figure 6a).

One notable departure from the myogenesis experimental workflow is the comparison between media supplementation and substrate adsorption. While we determined the adsorbed quantity of IT for myogenesis, the initial loading quantities of several established osteogenic factors are too low for accurate quantification. Therefore, media supplementation was conducted with the full, initial loading quantity of osteogenic factors.

To study osteogenesis of C2C12 cells, we optimized three factors known to enhance osteogenesis: (1) dexamethasone (DEX), a small hydrophobic molecule (Figure S12), (2) fibronectin, a multi-subunit protein (Figure S13), and (3) BMP2, a peptide.[42−44] All three differentiation factors were individually tested to verify their ability to enhance osteogenesis when adsorbed onto substrates compared to media supplementation (Figure S14). Notably, preliminary experiments found that DEX adsorption enhanced osteogenesis in MnO_2-coated substrates, not in GO-coated substrates (Figure S12). This result contrasts with C2C12 myogenesis, where both GO- and MnO_2-coated substrates enhanced differentiation. We hypothesize that this discrepancy is due to the mode of action between DEX and IT. DEX requires uptake by cells to stimulate osteogenesis, therefore requiring release from

https://doi.org/10.1021/acsami.2c10288
ACS Appl. Mater. Interfaces 2022, 14, 34488−34501

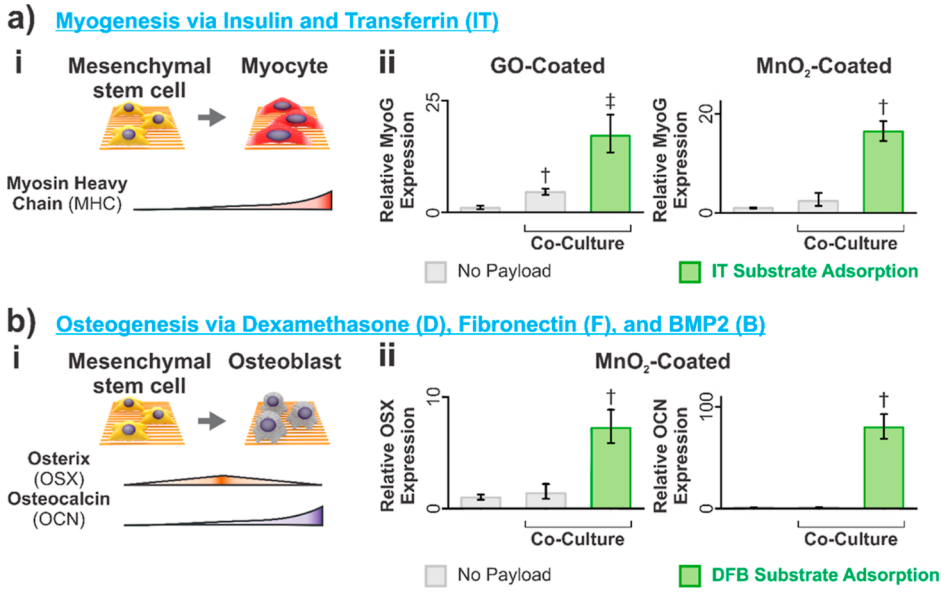

Figure 7. Spatially distinct co-culture subpopulations can be created using payload-adsorbed nanomaterial−nanofiber composite scaffolds. (a,b-i) Schematic diagram illustrating expression patterns for myogenesis and osteogenesis. (a-i) As cells undergo myogenesis to form myocytes, Myogenin expression increases. (b-ii) In contrast, cells undergoing osteogenesis transiently express OSX as intermediate pre-osteoblasts and OCN as terminally differentiated osteoblasts. Myogenesis (a-ii) and osteogenesis (b-ii) characterization via RT-qPCR reveals that C2C12 seeded on scaffolds with adsorbed differentiation factors undergoes significant differentiation, while C2C12 scaffolds without adsorbed payloads undergo modest to negligible differentiation even when co-cultured. RT-qPCR was analyzed using one-way ANOVA followed by Tukey's HSD within each nanomaterial group and measured gene [$\alpha = 0.05$; †, ‡, and ∼ indicate a statistically significant difference against all other conditions with different symbols, $n = 3$ biological replicates].

the substrate.[38] In contrast, IT are proteins that can bind to cell surface receptors (i.e., do not require uptake and remain active when bound to a surface), so drug release is not needed to induce myogenesis.[31,32] GO does not degrade (Figure 4a) and therefore does not release DEX. Conversely, MnO_2 biodegrades under physiological conditions to release payloads for cellular uptake. Considering these results, we selected only MnO_2-coated substrates for subsequent experiments.

With payload−nanomaterial compatibilities optimized and concentrations determined, combinations of DEX, fibronectin, and BMP2 (DFB) were supplemented into the media or adsorbed onto nanomaterial−nanofiber composite scaffolds. Conditions with "Media Supplementation" show increased OSX expression and relatively low OCN, indicating a high population of pre-osteoblasts (Figure 6b).[42] This result contrasts with the "Substrate Adsorption" cohort, which shows a more significant proportion of terminal osteoblasts, as evidenced by decreased OSX and increased OCN. This effect is mirrored in ICC staining, where DFB adsorbed onto MnO_2-coated nanofibers induces more C2C12 to become OCN-positive (Figure 6c).

As seen with C2C12 myogenesis, adsorbing differentiation factors onto hybrid scaffolds significantly increased the potency of payloads compared to conventional media supplementation. The advantages of the nanomaterial composite scaffold paradigm can be exploited for multi-lineage tissue regeneration. In addition, all three differentiation factors can be combined on a single substrate to achieve enhanced OCN expression. This result indicates that complex, heterogeneous solutions of differentiation factors are compatible with hybrid nanomaterial composite scaffolds.

2.5. Spatially Defined Co-Culture Systems Derived from a Single Cell Population. Another key aspect of our hybrid nanomaterial composite scaffold platform is the spatial control of differentiation. When inducing differentiation for tissue regeneration, spatial control over payload distribution and subsequent cell activity is of utmost importance for reducing off-target effects and controlling the organization of stem and differentiated cells.[45,46] A co-culture system was adopted to demonstrate this key advantage where two substrates, one with adsorbed payloads and one without, were cultured in the same well. IT and DFB solutions (as previously described in Sections 2.4.1 and 2.4.2) were employed to induce myogenesis and osteogenesis, respectively. Co-cultured cells were then compared to stem cells seeded on two substrates, both without adsorbed payloads in the same differentiation media. RT-qPCR markers previously described in Sections 2.4.1 and 2.4.2 were used here to determine the extent of differentiation (Figure 7a,b-i).

Despite co-culture with a shared volume of media, cells on different scaffolds showed different cell fates after 1 week. For both myogenesis and osteogenesis, cells on co-cultured scaffolds without adsorbed differentiation factor payloads ("No Payload" in the "Co-Culture" cluster) showed negligible difference compared to control cells cultured in wells without any media-supplemented or substrate-adsorbed payload (standalone "No Payload", Figure 7a,b-ii). In contrast, co-cultured scaffolds with adsorbed IT or DFB ("IT/DFB on Substrate" in the "Co-Culture" cluster) were able to induce myogenesis and osteogenesis, respectively.

As expected, scaffolds with adsorbed payloads (i.e., "IT/DFB on Substrate") continued to show enhanced stem cell differentiation even when co-cultured in the presence of additional cells seeded on "No Payload" scaffolds. Additionally, cells on "No Payload" scaffolds were largely unaffected by the presence of the adsorbed differentiation factors on "IT/DFB on Substrate" samples. This result suggests that the adsorbed payloads are unable to reach cells on "No Payload" scaffolds.

https://doi.org/10.1021/acsami.2c10288
ACS Appl. Mater. Interfaces 2022, 14, 34488−34501

The proposed mechanism for enhanced co-culture is thus as follows: stem cells seeded locally on "IT/DFB on Substrate" samples come into contact with adsorbed differentiation factors (via a reverse uptake mechanism), while cells seeded on the "No Payload" scaffold experience a significantly reduced payload concentration.[41]

With this proof of concept, co-culture systems with distinct, spatially discrete subpopulations derived from a common stem cell line can be easily generated by seeding cells on composite scaffolds with adsorbed differentiation factor payloads. These results demonstrate the ability of our nanomaterial composite scaffold to control differentiation in a spatially defined manner with minimized off-target effects (i.e., reduced differentiation on scaffolds without adsorbed payloads). For the in vitro study, hybrid nanomaterial composite scaffolds permit spatially organized co-culture systems that are difficult with conventional bulk media supplementation. Additional technologies such as dip-pen lithography and microcontact printing can be explored in subsequent studies to enhance the resolution and complexity of hybrid nanomaterial composite scaffold co-culture systems.[47,48] Future in vivo studies could leverage this enhanced spatial control over payload delivery to minimize off-target effects from bioactive payloads, such as ectopic bone growth from BMP2, on surrounding tissue.

2.6. Demonstration of Modularity with Human Patient-Derived Mesenchymal Stem Cells. While C2C12 cells are an established cell line for studying musculoskeletal injuries, the murine and spontaneous immortalization origin of the cell limits their ability to model human musculoskeletal regeneration. To develop a more clinically relevant tissue regeneration therapy model, autologous (human) primary cells are ideal to minimize risk for immunological reactions, genetic mutations during extended in vitro culture, and spontaneous transformation (i.e., decoupling from cell cycle regulatory mechanisms).[1,2,49] Primary human adipose-derived mesenchymal stem cells (ADSCs) were selected for this proof-of-concept demonstration of musculoskeletal injury regeneration. Moreover, the use of another cell line further demonstrates the modularity and broad suitability of the nanomaterial composite scaffold paradigm for various target applications.

MnO_2-coated nanofibers were exclusively used for their wider compatibility with a greater variety of payloads. Additionally, numerous government agencies (e.g., the United States FDA and United Kingdom Medicines and Healthcare Products Regulatory Agency) express concerns for the long-term in vivo effects of GO, representing significant regulatory and safety barriers to GO-coated nanofibers.[50]

2.6.1. Induction of Myogenesis in ADSCs. First, ADSCs were induced to undergo myogenesis (Figure S15). In contrast with the previous sections with C2C12, MyoG (late myocyte marker) and MyoD (intermediate myoblast marker) were both assayed via RT-qPCR since proliferative ADSCs do not innately express appreciable quantities of MyoG or MyoD.[40]

Since IT are found in the basal media (α-MEM) supporting ADSCs during proliferation, other myogenic factors were used. Preliminary experiments revealed that DEX enabled myogenesis rather than osteogenesis. Literature reports elsewhere detail differential effects of DEX on different stem cell lines at different stages of differentiation.[51,52] ADSCs cultured without media supplementation or substrate-adsorbed payload ("No Payload" cluster) were used to normalize MyoG expression, while ADSCs cultured in DEX-supplemented media ("DEX Media Supplementation") were used to normalize MyoD expression. MnO_2-coated nanofibers with adsorbed DEX ("DEX Substrate Adsorption") were able to induce myogenesis in ADSCs, albeit to a lesser extent than to which IT-adsorbed substrates were able to induce myogenesis in C2C12 (Figures S15 and 5b). RT-qPCR reveals statistically significant upregulation in MyoD, indicating a greater proportion of myoblasts on substrates with adsorbed DEX. Interestingly, MyoG was also upregulated, though not to a statistically significant degree. These results were corroborated with ICC staining, where ADSCs exhibit stronger MHC fluorescence on DEX-adsorbed scaffolds than for media supplementation.

As seen in C2C12 myogenesis, the nanomaterial–nanofiber composite scaffold performs optimally when using the nanomaterial-mediated enhanced loading capacity to adsorb the myogenic payload onto the scaffold. We presume that the mechanism for this myogenesis enhancement remains the same, that is, adsorbing the differentiation factor increases the local concentration for the intended recipient ADSCs compared to media supplementation. With this demonstration, myogenesis can be induced in more than one cell line, increasing the versatility of the nanomaterial composite scaffold.

2.6.2. Induction of Osteogenesis in ADSCs. To further demonstrate the utility of this technique as a modular platform technology, ADSCs were also induced to undergo osteogenesis using only fibronectin and BMP2 (Figure S16, FB). ADSCs cultured in proliferative media failed to express OSX (intermediate osteogenesis marker) and OCN (late osteogenesis marker), so ADSCs cultured without media supplementation or substrate adsorption ("No Payload") were used to normalize expression for OSX and OCN. For the control of osteogenesis, adsorption of FB onto MnO_2-coated nanofibers ("FB Substrate Adsorption") was sufficient to induce a nearly 8-fold increased OCN expression compared to "No Payload" samples (Figure S16). Conversely, bulk media supplementation with FB ("FB Media Supplementation") failed to produce a significant change in OCN expression. This osteogenesis enhancement pattern is also seen in ICC images where a greater proportion of ADSCs are OCN-positive on the FB-adsorbed scaffold than on FB-supplemented media.

With this demonstration of enhanced osteogenesis and myogenesis across both C2C12 and ADSC cultures, we have verified that the nanomaterial–nanofiber composite scaffold system exhibits broad applicability for tissue engineering applications. Both myogenic and osteogenic payloads can be adsorbed onto the scaffold to increase stem cell differentiation efficacy, indicating the potential to generate multiple cell types from a single parent cell population. Moreover, different cell lines respond similarly well to the payload-adsorbed scaffold, allowing clinicians to reliably apply this technology to different patients and their derived stem cells.

3. CONCLUSIONS

Taken together, we have developed a hybrid nanomaterial–nanofiber composite scaffold system that allows for a precisely fabricated nanotopography without sacrificing soluble factor bioactivity during harsh manufacturing steps. Both GO and MnO_2 significantly increased payload adsorption compared to conventional, bare porous scaffolds. Whereas physical adsorption on conventional, porous scaffolds suffers from uncontrolled burst release, GO-coated scaffolds maximized drug retention, while MnO_2-coated scaffolds displayed cell-

https://doi.org/10.1021/acsami.2c10288
ACS Appl. Mater. Interfaces 2022, 14, 34488–34501

responsive biodegradation and drug release. When differentiation factors were adsorbed on nanomaterial−nanofiber composite scaffolds, stem cells experienced enhanced differentiation efficiency compared to conventional media supplementation. This technology was then extended for spatial control over differentiation. When multiple nanomaterial-coated scaffolds (with and without adsorbed payloads) were co-cultured in the same well, only cells seeded on payload-adsorbed scaffold displayed enhanced differentiation. Because of these unique features, we believe that our technology will be beneficial for the field of regenerative medicine and can be applied to a variety of other systems outside of musculoskeletal injuries.

4. MATERIALS AND METHODS

4.1. Materials. The SYBR Green PCR Master Mix was purchased from Applied Biosystems. Sodium hydroxide (NaOH) was purchased from Chem Impex. 25 × 25 mm glass coverslips, six-well plates, nonbinding 96-well plates, polyethersulfone membrane vacuum filter systems (0.22 μm pore size), and Dulbecco's modified Eagle medium (DMEM) were purchased from Corning. Copper TEM grids and carbon tape were purchased from Electron Microscopy Sciences. Silicone adhesive was purchased from Factor II. Ethyl acetate, aluminum foil, glutaraldehyde solution (50% w/w), and an Accumet pH meter were purchased from Fisher Scientific. Dulbecco's phosphate-buffered saline (DPBS), bone morphogenetic protein 2 (BMP2), fibronectin, FBS, penicillin−streptomycin (Pen-Strep), trypsin−EDTA, TrypLE Express, horse serum (HS), and minimum essential medium α were purchased from Gibco. Non-adherent six-well plates were purchased from Greiner Bio-One. The human insulin ELISA kit, TRIzol reagent, SuperScript III first-strand synthesis system, mouse anti-MHC, goat anti-Rabbit IgG Alexa Fluor 488, goat anti-Mouse IgG Alexa Fluor 546, and Hoechst 33342 solution were purchased from Invitrogen. KimWipe sheets were purchased from Kimberly-Clark Professional. Folded capillary cells were purchased from Malvern. Glycine and DEX were purchased from MP Biomedicals. Amine-functionalized sensors were purchased from Nicoya LifeSciences. 30-gauge blunt needles were purchased from Nordson EFD. Parafilm was purchased from Pechiney Plastic Packaging. Rabbit anti-osteocalcin (for staining human cells) was purchased from ProteinTech. Rabbit anti-myogenin was purchased from Santa Cruz Biotech. Gelatin type B from bovine skin, acetic acid, ascorbic acid, BSA, ethylene glycol, urea, magnesium chloride ($MgCl_2$), hydrochloric acid (HCl), insulin solution, transferrin, PLTMax human platelet lysate, (+)-α-tocopherol acetate, Trypan Blue, formalin solution (10%), and rabbit anti-osteocalcin (for staining mouse cells) were purchased from Sigma-Aldrich. SEM specimen stubs were purchased from Ted Pella. Spectrophotometer cuvettes were purchased from VWR.

4.2. GO and MnO_2 Nanosheet Characterization. GO and MnO_2 nanosheets were synthesized as reported in the previous literature. In-depth protocols can be found in the Supporting Information.

GO and MnO_2 nanosheet solutions were diluted to 1 μg mL^{-1} prior to filling spectrophotometer cuvettes and folded capillary cells for dynamic light scattering and zeta potential measurements using a ZetaSizer Nano NS (Malvern) instrument.

TEM samples were prepared by drop-casting GO or MnO_2 nanosheet solutions (1 μg mL^{-1}, 10 μL) onto copper TEM grids. The solution was allowed to dry completely overnight before imaging using a Philips CM12 TEM (FEI).

XPS samples were prepared by drop-casting GO or MnO_2 nanosheet solutions (1 mg mL^{-1}, 40 μL) onto silicon wafers. The solution was allowed to dry completely overnight before measurement using a K-Alpha X-ray photoelectron spectrophotometer (Thermo Fisher).

4.3. Gelatin Nanofiber Electrospinning. Gelatin nanofibers were electrospun using a slight variation on a reported protocol.[22] Gelatin type B from bovine skin (0.4053 g), ethyl acetate (1.395 mL), acetic acid (1.89 mL), and deionized water (0.9 mL) were mixed and sonicated for 1 h prior to loading into the electrospinning apparatus (NanoNC). A 9 cm rotating mandrel (2000 revolutions per minute) was covered with aluminum foil and positioned 10 cm away from the tip of the syringe needle. The solution was set to flow (0.14 mL h^{-1}) through a 30-gauge blunt needle, and a power supply (Gamma high voltage) was used to establish an electric potential difference (20 kV) between the needle tip and grounded mandrel. A mat of gelatin nanofibers was collected for 6 h.

4.4. Bare/GO-/MnO_2-Coated Gelatin Nanofiber Preparation. A 25 × 25 mm glass coverslip was lightly coated with silicone adhesive and allowed to dry while covered. Gelatin nanofibers were transferred from the aluminum foil onto the glass support substrate. Transferred gelatin nanofibers were placed in a polystyrene dish with a central reservoir of glutaraldehyde solution. The dish was sealed with Parafilm, and the glutaraldehyde vapor crosslinked the gelatin nanofibers over the course of 2 days at ambient temperature and pressure.

For nanomaterial adsorption, GO or MnO_2 nanosheet solutions (1 mg mL^{-1}, 1 mL) were spread across the bottom of a single well of a six-well plate. Crosslinked gelatin nanofibers were placed fiber side down onto the GO or MnO_2 nanosheet solutions. The well plate was sealed with Parafilm, and the GO/MnO_2 nanosheets adsorbed onto the gelatin nanofibers overnight. Excess GO/MnO_2 nanosheet solution was blotted off using a KimWipe sheet. GO-/MnO_2-coated gelatin nanofibers were dried overnight at ambient conditions.

Bare gelatin nanofiber scaffolds were prepared in the same manner using deionized water instead of GO/MnO_2 nanosheet solutions.

For co-culture experiments, 25 × 25 mm glass coverslips were cut in half using a diamond-tip stylus to yield two 25 × 12.5 mm halves. Subsequent GO-/MnO_2-coated gelatin nanofiber preparation steps were performed with each pair maintained together (e.g., each pair was placed in the same GO/MnO_2 nanosheet adsorption well).

4.5. Bare/GO-/MnO_2-Coated Gelatin Nanofiber Characterization. Bare/GO-/MnO_2-coated gelatin nanofiber samples for FE-SEM and energy-dispersive X-ray spectroscopy (EDS) were mounted on an SEM specimen stub using carbon tape before being placed in a desiccator cabinet overnight. Desiccated samples were sputter-coated with either gold (20 nm thickness) or carbon (5 nm thickness) using an EMS150T ES sputter coater (Quorum Technologies).

Gold-sputtered samples were placed in a Sigma FE-SEM instrument (Carl Zeiss AG) with the accelerating voltage set to under 5 kV to prevent charging and sample damage. A secondary electron detector (SE2) was used to form images. ImageJ was used to crop out extraneous system information and recreate scale bars.

Carbon-sputtered samples were placed in the above Sigma FE-SEM instrument fitted with an INCA PentraFETx3 EDS detector (Oxford Instrument). The electron beam was set to 15 kV and used to probe elemental composition.

For Raman spectroscopy, bare/GO-/MnO_2-coated gelatin nanofibers were placed in a desiccator cabinet overnight before measurement using an inVia Raman microscope (Renishaw) with a 633 nm laser. Autofluorescence background was corrected using the Vancouver Raman algorithm in MATLAB.

For contact angle measurement, bare/GO-/MnO_2-coated gelatin nanofiber samples were placed on a level, homemade stage in a darkened room. A camera was positioned so the sample was centered and level within the image field of view. Deionized water (10 μL) was pipetted onto the sample, and a flashlight was positioned behind the camera to enhance the contrast of the water droplet. The contact angle was determined with the aid of CorelDraw.

4.6. FITC-Labeled Protein Loading Quantification. Individual solutions of FITC-labeled gelatin type A, BSA, and lysozyme were diluted in sterile water to a concentration of 15.5 μg mL^{-1}. To test FITC−insulin adsorption, stock transferrin (not FITC-labeled) was diluted to 5.5 μg mL^{-1} and FITC−insulin solution was diluted to 10 μg mL^{-1}. To test FITC−transferrin, stock insulin was diluted to 10 μg mL^{-1} and FITC−transferrin solution was diluted to 5.5 μg mL^{-1}. FITC-labeled gelatin, BSA, lysozyme, insulin, or transferrin solutions

https://doi.org/10.1021/acsami.2c10288
ACS Appl. Mater. Interfaces 2022, 14, 34488−34501

(1 mL) were adsorbed onto bare/GO-/MnO_2-coated gelatin nanofiber samples overnight in a humidified incubator (37 °C, 5% CO_2). Afterward, each sample was washed three times using sterile water (2 mL per washing); each washing solution was collected for non-adsorbed FITC protein analysis.

Collected FITC protein washing supernatants and a standard curve (15.5 to 0 $\mu g\ mL^{-1}$) were pipetted in the non-binding 96-well plate in triplicate. Fluorescence was assayed using an Infinite M200 Pro (Tecan) instrument at λ_{ex} = 488 nm and λ_{em} = 525 nm. The concentration was calculated from an Akima spline interpolation curve to account for non-linearity at lower concentrations.

Statistical analysis for each FITC-labeled protein was performed on supernatant fluorescence readings using a one-tailed Dunnett's test against the no-GO/MnO_2 nanosheet condition using built-in R (statistical computer language) functions.

4.7. Protein Release Quantification. *4.7.1. SPR Characterization.* Short-term (seconds to minutes) BSA release was assayed using SPR.

Ascorbic acid solutions (1 mg mL^{-1} and 10 $\mu g\ mL^{-1}$) and BSA (1 mg mL^{-1}, SPR BSA) solutions were synthesized with deionized water and stored for no more than 1 week at 4 °C.

Regeneration solutions [i.e., glycine (10 mM, pH 1.5), NaOH (0.2 M, pH 13.3), ethylene glycol (50% w/w, pH 10), urea (8 M), and $MgCl_2$ (4 M)] were adjusted with HCl (1 M) or NaOH (1 M) and monitored using a pH meter (Fisher Scientific) until the desired pH was achieved.

GO and MnO_2 solutions (1 mg mL^{-1}, 0.15 mL) were slowly added to HCl (100 μM, 0.85 mL) to yield GO or MnO_2 nanosheet SPR solution. Due to MnO_2 tendency to precipitate in acidic solutions over extended periods of time, GO/MnO_2 nanosheet SPR solutions were used within 4 h of mixing.

Amine-functionalized sensors were washed with deionized water before loading into an OpenSPR instrument (Nicoya LifeSciences). Sensors were activated with HCl (85 μM, flow: 150 $\mu L\ min^{-1}$, 25 s), coated with GO/MnO_2 nanosheet SPR solutions (20 $\mu L\ min^{-1}$, 218 s), blocked with 1 M acetic acid (20 $\mu L\ min^{-1}$, 218 s), treated with SPR BSA solution (20 $\mu L\ min^{-1}$, 218 s), and challenged with various regeneration solutions (100 $\mu L\ min^{-1}$, 38 s).

4.7.2. ELISA Characterization. Long-term (hours to weeks) insulin release was assayed using ELISA.

Insulin (10 $\mu g\ mL^{-1}$, not FITC-labeled) was adsorbed onto GO- and MnO_2-coated gelatin nanofibers as specified in the section "*Protein Loading Quantification*". During this time, wells of a non-adherent six-well plate were blocked with BSA in DPBS (1% w/v) overnight in a humidified incubator to prevent nonspecific adsorption of insulin.

Insulin-loaded bare/GO-/MnO_2-coated gelatin nanofibers were transferred to the blocked wells after washing. DPBS, FBS, or DPBS with ascorbic acid (1 $\mu g\ mL^{-1}$) was added to each well (3 mL) before Parafilm sealing and placement on a rotary shaker (40 RPM) in a humidified incubator. Aliquots were taken at predetermined times (i.e., 1 h, 1 day, 3 days, 7 days, and 14 days) without replacement and stored in a freezer (−80 °C). Each aliquot was subjected to exactly one freeze−thaw cycle before assaying using a human insulin ELISA kit as per the manufacturer's instructions.

4.8. Differentiation Factor Adsorption. Differentiation factor (i.e., insulin, transferrin, DEX, fibronectin, and BMP2) absorption followed a similar protocol to that described above in Section 4.6 "*FITC-Labeled Protein Loading Quantification*".

Insulin solution did not require further modifications prior to dilution for adsorption. Transferrin was reconstituted with minor modifications to the manufacturer's instructions. The lyophilized powder was reconstituted in DPBS to a concentration of 2.5 mg mL^{-1}.

BMP2 was reconstituted with minor modifications to the manufacturer's instructions. The lyophilized powder was reconstituted in 20 mM acetic acid to a concentration of 0.1 mg mL^{-1}. The solution was further diluted with BSA in deionized water (0.5 mg mL^{-1}) to a final concentration of 10 $\mu g\ mL^{-1}$ BMP2. Fibronectin was reconstituted in deionized water to a final concentration of 1 mg mL^{-1}. DEX was dissolved in ethanol to a final concentration of 10 μM.

Bare/GO-/MnO_2-coated gelatin nanofibers were placed in wells of a non-adherent six-well plate and UV-sterilized (15 min) prior to differentiation factor adsorption.

Stock insulin (0.1% v/v), transferrin (0.22% v/v), and BMP2 (2% v/v) solutions were diluted in sterile water at fixed ratios for substrate adsorption onto bare/GO-/MnO_2-coated gelatin nanofiber samples. After initial optimization experiments (Figures S12 and S13) using various test concentrations, subsequent stem cell differentiation experiments (Figures 6, 7, S14, and S16) used stock DEX (0.2% v/v) and fibronectin (1% v/v) solutions diluted in sterile water at fixed ratios.

After differentiation factor cocktails were mixed at the desired dilutions in sterile water, the solutions were pipetted (1 mL for 25 × 25 mm and 0.5 mL for 25 × 12.5 mm bare/GO-/MnO_2-coated gelatin nanofibers) to cover the samples. The differentiation factors were adsorbed overnight in a humidified incubator (37 °C, 5% CO_2). Bare/GO-/MnO_2-coated gelatin nanofibers were washed three times using sterile water (2 mL per washing) and placed in a fresh well.

4.9. Cell Culture. Various media were mixed and vacuum filtration sterilized through a polyethersulfone membrane. C2C12 proliferation media consisted of FBS (10% v/v), Pen-Strep (1% v/v), and DMEM. ADSC proliferation media consisted of PLTMax human platelet lysate (10% v/v) and minimum essential medium α. A (+)-α-tocopherol acetate in ethanol solution (10% w/w) was used to supplement ADSC proliferation media (1:1000 dilution) immediately before cell culture. Basal myogenesis media consisted of HS (2% v/v), Pen-Strep (1% v/v), and DMEM. Basal osteogenesis media consisted of FBS (5% v/v), Pen-Strep (1% v/v), and DMEM.

When comparing adsorbed IT to equivalent media supplementation [that is, "IT in media" samples in (Figure 4) and "Equiv IT in media" samples in (Figure S11)] for C2C12 myogenesis, stock IT solutions were used as supplements in basal myogenesis media (2 mL) in accordance with the quantities determined via "*FITC-Labeled Protein Loading Quantification*" procedures. Specific concentration and dilution values can be found in Table S1.

When investigating literature-recommended media supplementation concentrations that exceed bare/GO-/MnO_2-coated gelatin nanofiber loading capacity [that is, "Full IT in Media" in (Figure S11)], stock insulin (0.05% v/v, 10 μg) and transferrin (0.11% v/v, 5.5 μg) solutions were added to basal myogenesis media (2 mL) in accordance with previous reports.

For C2C12 myogenesis and ADSC myogenesis/osteogenesis, stock DEX (0.1% v/v, 0.02 nmol), fibronectin (0.5% v/v, 10 μg), and BMP2 (1% v/v, 200 ng) were diluted in basal myogenesis or osteogenesis media (2 mL) at literature-recommended media supplementation concentrations. No corrections were made to normalize to the substrate loading capacity.

C2C12 (ATCC) was used between passages 15−20 since receiving. Care was taken to ensure that the cells did not exceed 80% confluency during propagation. ADSCs (American CryoStem) were used between passages 5 and 10 since receiving and cultured on fibronectin-treated plasticware before use with bare/GO-/MnO_2-coated gelatin nanofibers. Cells were delaminated and collected for seeding onto bare/GO-/MnO_2-coated gelatin nanofibers via trypsin−EDTA for C2C12 and TrypLE Express for ADSCs. Viable cell counts were determined via Trypan Blue exclusion.

Each bare/GO-/MnO_2-coated gelatin nanofiber sample was placed in an individual well of a non-adherent six-well plate.

For C2C12, each well was seeded with cells suspended in DMEM (100,000 cells mL^{-1}, 2 mL). After 2 hours, seeded bare/GO-/MnO_2-coated gelatin nanofibers were transferred to another well with appropriate basal or supplemented differentiation media (2 mL). Control proliferation wells had DMEM aspirated and replaced with proliferation media. Cells were treated with the TRIzol reagent or formalin solution on day 7.

For co-culture experiments, individual halves of each co-culture pair were seeded with cells in separate wells, as described before. After

https://doi.org/10.1021/acsami.2c10288
ACS Appl. Mater. Interfaces 2022, 14, 34488−34501

2 h, corresponding co-culture pairs were brought together in the same well for culture. Cells were treated with the TRIzol reagent on day 7.

For ADSC, each well was seeded with cells suspended in ADSC proliferation media (100,000 cells mL^{-1}, 2 mL). After 2 hours, seeded bare/GO-/MnO_2-coated gelatin nanofibers were transferred to another well with transition media (50% v/v ADSC proliferation media in basal differentiation media). Control proliferation wells had DMEM aspirated and replaced with proliferation media. After 24 h, each sample was transferred to another well with appropriate basal or supplemented differentiation media. After 7 days, additional basal differentiation media (1 mL) were added to each well. Cells were treated with the TRIzol reagent or formalin solution on day 14.

RT-qPCR was performed on TRIzol-extracted mRNA using the manufacturer-suggested protocols for the SuperScript III first-strand synthesis system and SYBR Green PCR Master Mix. Primer sequences can be found in Table S2. Formalin-fixed cells were immunostained using the following antibodies: mouse anti-myosin heavy chain (1:500), rabbit anti-myogenin (1:100), rabbit anti-osteocalcin (human cells—1:200, mouse cells—1:100), goat anti-rabbit IgG Alexa Fluor 488 (1:200), goat anti-mouse IgG Alexa Fluor 546 (1:200), and Hoechst 33342 (0.1 mg mL^{-1}).

4.10. Computer Software. OriginLab was used for data analysis and graphing unless specified elsewhere. Blender was used to generate select graphics. CorelDraw was used for figure generation.

4.11. Statistical Analysis. ANOVA with Tukey's HSD post hoc testing was performed for RT-qPCR results using MATLAB [α = 0.05, * indicates a statistically significant difference; †, ‡, and ~ indicate a statistically significant difference against all other conditions with different symbols, n = 3]. ANOVA with Dunnett's Test post hoc analysis was performed for cytotoxicity (Figure S10) and FITC protein loading capacity results using R (statistical software) [α = 0.05, the symbol indicates a statistically significant difference against 0 μg mL^{-1} GO or MnO_2 nanosheet solution (cytotoxicity) or bare gelatin nanofibers (FITC protein adsorption), n = 3].

■ ASSOCIATED CONTENT

Supporting Information

The Supporting Information is available free of charge at https://pubs.acs.org/doi/10.1021/acsami.2c10288.

Additional experimental materials and methods; FESEM, TEM, DLS, zeta potential, AFM, and contact angle characterization of nanofibers, GO, and MnO_2; removal of weakly adsorbed payloads; optimization of BSA and nanomaterial adsorption/desorption on SPR sensors; additional C2C12 myogenesis RT-qPCR controls; osteogenic differentiation factor concentration optimization; and ADSC myogenesis/osteogenesis (PDF)

■ AUTHOR INFORMATION

Corresponding Author

Ki-Bum Lee − *Department of Chemistry and Chemical Biology, Rutgers University, Piscataway, New Jersey 08854, United States;* orcid.org/0000-0002-8164-0047; Phone: +1-848-445-2081; Email: kblee@rutgers.edu; https://kblee.rutgers.edu/

Authors

Jeffrey Luo − *Department of Chemistry and Chemical Biology, Rutgers University, Piscataway, New Jersey 08854, United States;* orcid.org/0000-0002-0140-1370

Letao Yang − *Department of Chemistry and Chemical Biology, Rutgers University, Piscataway, New Jersey 08854, United States;* orcid.org/0000-0002-0572-9787

Sy-Tsong Dean Chueng − *Department of Chemistry and Chemical Biology, Rutgers University, Piscataway, New Jersey 08854, United States;* orcid.org/0000-0002-1447-5491

Brian Conley − *Department of Chemistry and Chemical Biology, Rutgers University, Piscataway, New Jersey 08854, United States*

Christopher Rathnam − *Department of Chemistry and Chemical Biology, Rutgers University, Piscataway, New Jersey 08854, United States;* orcid.org/0000-0003-3111-4687

Complete contact information is available at: https://pubs.acs.org/10.1021/acsami.2c10288

Author Contributions

B.C. and C.R. contributed equally to this paper. **J.L.**: conceptualization, methodology, software, validation, formal analysis, investigation, resources, data curation, writing—original draft, writing—review and editing, visualization, and funding acquisition. **L.Y.**: conceptualization, methodology, writing—review and editing, and visualization. **S.-T.D.C.**: conceptualization, resources, writing—review and editing, visualization, and funding acquisition. **B.C.**: methodology, investigation, and writing—review and editing. **C.R.**: methodology, investigation, writing—review and editing, and funding acquisition. **K.-B.L.**: writing—review and editing, supervision, project administration, and funding acquisition.

Notes

The authors declare no competing financial interest.

■ ACKNOWLEDGMENTS

K.-B.L. acknowledges the financial support from the NSF (CBET-1803517), the New Jersey Commission on Spinal Cord (CSCR17IRG010 and CSCR22ERG023), NIH R21 (R21AR071101), and NIH R01 (1R01DC016612, 3R01DC016612-01S1, and 5R01DC016612-02S1). J.L. acknowledges the financial support from the NIH T32 Biotechnology Training Fellowship (GM008339). The authors would like to acknowledge Dr. Adam J. Gormley for assistance with SPR, Dr. Sagar D. Khare for assistance with microplate photometers, and Yannan Hou for assistance with Raman spectroscopy.

■ REFERENCES

(1) Atala, A.; Lanza, R.; Mikos, T.; Nerem, R. *Principles of Regenerative Medicine*; Academic Press, 2018.

(2) Loebel, C.; Burdick, J. A. Engineering Stem and Stromal Cell Therapies for Musculoskeletal Tissue Repair. *Cell Stem Cell* **2018**, *22*, 325−339.

(3) Li, J.; Mooney, D. J. Designing Hydrogels for Controlled Drug Delivery. *Nat. Rev. Mater.* **2016**, *1*, 1−17.

(4) Ji, W.; Sun, Y.; Yang, F.; van den Beucken, J. J.; Fan, M.; Chen, Z.; Jansen, J. A. Bioactive Electrospun Scaffolds Delivering Growth Factors and Genes for Tissue Engineering Applications. *Pharm. Res.* **2011**, *28*, 1259−1272.

(5) Pham, Q. P.; Sharma, U.; Mikos, A. G. Electrospinning of Polymeric Nanofibers for Tissue Engineering Applications: A Review. *Tissue Eng.* **2006**, *12*, 1197−1211.

(6) Liu, X.; Zhou, Y.; Xie, W.; Liu, S.; Zhao, Q.; Huang, W. Construction of Smart Manganese Dioxide-Based All-in-One Nanoplatform for Cancer Diagnosis and Therapy. *Small Methods* **2020**, *4*, 2000566.

(7) Palmer, D.; Levina, M.; Douroumis, D.; Maniruzzaman, M.; Morgan, D. J.; Thomas P Farrell, T. P.; Rajabi-Siahboomi, A. R.; Nokhodchi, A. Mechanism of Synergistic Interactions and Its Influence on Drug Release from Extended Release Matrices

Manufactured Using Binary Mixtures of Polyethylene Oxide and Sodium Carboxymethylcellulose. *Colloids Surf., B* **2013**, *104*, 174−180.
(8) Geetha, P.; Sivaram, A. J.; Jayakumar, R.; Gopi Mohan, C. G. Integration of in Silico Modeling, Prediction by Binding Energy and Experimental Approach to Study the Amorphous Chitin Nanocarriers for Cancer Drug Delivery. *Carbohydr. Polym.* **2016**, *142*, 240−249.
(9) Chueng, S.-T. D.; Yang, L.; Zhang, Y.; Lee, K.-B. Multidimensional Nanomaterials for the Control of Stem Cell Fate. *Nano Convergence* **2016**, *3*, 1−15.
(10) Sanchez, V. C.; Jachak, A.; Hurt, R. H.; Kane, A. B. Biological Interactions of Graphene-Family Nanomaterials: An Interdisciplinary Review. *Chem. Res. Toxicol.* **2012**, *25*, 15−34.
(11) Yang, L.; Kim, T. H.; Cho, H. Y.; Luo, J.; Lee, J. M.; Chueng, S. T. D.; Hou, Y.; Yin, P. T. T.; Han, J.; Kim, J. H.; Chung, B. G.; Choi, J. W.; Lee, K. B. Hybrid Graphene-Gold Nanoparticle-Based Nucleic Acid Conjugates for Cancer-Specific Multimodal Imaging and Combined Therapeutics. *Adv. Funct. Mater.* **2021**, *31*, 2006918.
(12) Wu, M.; Hou, P.; Dong, L.; Cai, L.; Chen, Z.; Zhao, M.; Li, J. Manganese Dioxide Nanosheets: From Preparation to Biomedical Applications. *Int. J. Nanomed.* **2019**, *14*, 4781.
(13) Yang, L.; Chueng, S.-T. D.; Li, Y.; Patel, M.; Rathnam, C.; Dey, G.; Wang, L.; Cai, L.; Lee, K.-B. A Biodegradable Hybrid Inorganic Nanoscaffold for Advanced Stem Cell Therapy. *Nat. Commun.* **2018**, *9*, 3174.
(14) Kumar, S.; Adjei, I. M.; Brown, S. B.; Liseth, O.; Sharma, B. Manganese Dioxide Nanoparticles Protect Cartilage from Inflammation-Induced Oxidative Stress. *Biomaterials* **2019**, *224*, 119467.
(15) Ding, Z.; Ma, H.; Chen, Y. Interaction of Graphene Oxide with Human Serum Albumin and Its Mechanism. *RSC Adv.* **2014**, *4*, 55290−55295.
(16) Makharza, S.; Vittorio, O.; Cirillo, G.; Oswald, S.; Hinde, E.; Kavallaris, M.; Büchner, B.; Mertig, M.; Hampel, S. Graphene Oxide-Gelatin Nanohybrids as Functional Tools for Enhanced Carboplatin Activity in Neuroblastoma Cells. *Pharm. Res.* **2015**, *32*, 2132−2143.
(17) Wan, C.; Frydrych, M.; Chen, B. Strong and Bioactive Gelatin−Graphene Oxide Nanocomposites. *Soft Matter* **2011**, *7*, 6159−6166.
(18) La, W. G.; Park, S.; Yoon, H. H.; Jeong, G. J.; Lee, T. J.; Bhang, S. H.; Han, J. Y.; Char, K.; Kim, B. S. Delivery of a Therapeutic Protein for Bone Regeneration from a Substrate Coated with Graphene Oxide. *Small* **2013**, *9*, 4051−4060.
(19) Lvov, Y.; Munge, B.; Giraldo, O.; Ichinose, I.; Suib, S. L.; Rusling, J. F. Films of Manganese Oxide Nanoparticles with Polycations or Myoglobin from Alternate-Layer Adsorption. *Langmuir* **2000**, *16*, 8850−8857.
(20) Cooper, G. M.; Hausman, R. E.; Hausman, R. E. *The Cell: A Molecular Approach*; ASM Press: Washington, DC, 2007; Vol. *4*.
(21) Mandal, A.; Clegg, J. R.; Anselmo, A. C.; Mitragotri, S. Hydrogels in the Clinic. *Bioeng. Transl. Med.* **2020**, *5*, No. e10158.
(22) Song, J.-H.; Kim, H.-E.; Kim, H.-W. Production of Electrospun Gelatin Nanofiber by Water-Based Co-Solvent Approach. *J. Mater. Sci.: Mater. Med.* **2008**, *19*, 95−102.
(23) Bancelin, S.; Aimé, C.; Gusachenko, I.; Kowalczuk, L.; Latour, G.; Coradin, T.; Schanne-Klein, M.-C. Determination of Collagen Fibril Size Via Absolute Measurements of Second-Harmonic Generation Signals. *Nat. Commun.* **2014**, *5*, 1−8.
(24) Sheets, K.; Wunsch, S.; Ng, C.; Nain, A. S. Shape-Dependent Cell Migration and Focal Adhesion Organization on Suspended and Aligned Nanofiber Scaffolds. *Acta Biomater.* **2013**, *9*, 7169−7177.
(25) Dang, J. M.; Leong, K. W. Myogenic Induction of Aligned Mesenchymal Stem Cell Sheets by Culture on Thermally Responsive Electrospun Nanofibers. *Adv. Mater.* **2007**, *19*, 2775−2779.
(26) Chen, X.; Fu, X.; Shi, J.-g.; Wang, H. Regulation of the Osteogenesis of Pre-Osteoblasts by Spatial Arrangement of Electrospun Nanofibers in Two-and Three-Dimensional Environments. *Nanomedicine (N.Y., NY, U.S.)* **2013**, *9*, 1283−1292.
(27) Prichard, H. L.; Reichert, W. M.; Klitzman, B. Adult Adipose-Derived Stem Cell Attachment to Biomaterials. *Biomaterials* **2007**, *28*, 936−946.
(28) Curran, J. M.; Chen, R.; Hunt, J. A. The Guidance of Human Mesenchymal Stem Cell Differentiation in Vitro by Controlled Modifications to the Cell Substrate. *Biomaterials* **2006**, *27*, 4783−4793.
(29) Phan, H. T.; Bartelt-Hunt, S.; Rodenhausen, K. B.; Schubert, M.; Bartz, J. C. Investigation of Bovine Serum Albumin (Bsa) Attachment onto Self-Assembled Monolayers (Sams) Using Combinatorial Quartz Crystal Microbalance with Dissipation (Qcm-D) and Spectroscopic Ellipsometry (Se). *PLoS One* **2015**, *10*, No. e0141282.
(30) Ouberai, M. M.; Xu, K.; Welland, M. E. Effect of the Interplay between Protein and Surface on the Properties of Adsorbed Protein Layers. *Biomaterials* **2014**, *35*, 6157−6163.
(31) Liu, S. Q.; Ito, Y.; Imanishi, Y. Cell Growth on Immobilized Cell Growth Factor: 5. Interaction of Immobilized Transferrin with Fibroblast Cells. *Int. J. Biol. Macromol.* **1993**, *15*, 221−226.
(32) Ito, Y.; Zheng, J.; Imanishi, Y.; Yonezawa, K.; Kasuga, M. Protein-Free Cell Culture on an Artificial Substrate with Covalently Immobilized Insulin. *Proc. Natl. Acad. Sci. U.S.A.* **1996**, *93*, 3598−3601.
(33) Du, J.; Cullen, J. J.; Buettner, G. R. Ascorbic Acid: Chemistry, Biology and the Treatment of Cancer. *Biochim. Biophys. Acta, Rev. Cancer* **2012**, *1826*, 443−457.
(34) Schasfoort, R. B. *Handbook of Surface Plasmon Resonance*; Royal Society of Chemistry, 2017.
(35) Sopotnik, M.; Leonardi, A.; Križaj, I.; Dušak, P.; Makovec, D.; Mesarič, T.; Ulrih, N. P.; Junkar, I.; Sepčić, K.; Drobne, D. Comparative Study of Serum Protein Binding to Three Different Carbon-Based Nanomaterials. *Carbon* **2015**, *95*, 560−572.
(36) Milani, S.; Baldelli Bombelli, F.; Pitek, A. S.; Dawson, K. A.; Rädler, J. Reversible Versus Irreversible Binding of Transferrin to Polystyrene Nanoparticles: Soft and Hard Corona. *ACS Nano* **2012**, *6*, 2532−2541.
(37) Noh, H.; Vogler, E. A. Volumetric Interpretation of Protein Adsorption: Competition from Mixtures and the Vroman Effect. *Biomaterials* **2007**, *28*, 405−422.
(38) Lee, K.-S.; Kim, H.-J.; Li, Q.-L.; Chi, X.-Z.; Ueta, C.; Komori, T.; Wozney, J. M.; Kim, E.-G.; Choi, J.-Y.; Ryoo, H.-M.; Bae, S.-C. Runx2 Is a Common Target of Transforming Growth Factor B1 and Bone Morphogenetic Protein 2, and Cooperation between Runx2 and Smad5 Induces Osteoblast-Specific Gene Expression in the Pluripotent Mesenchymal Precursor Cell Line C2c12. *Mol. Cell. Biol.* **2000**, *20*, 8783.
(39) Diokmetzidou, A.; Tsikitis, M.; Nikouli, S.; Kloukina, I.; Tsoupri, E.; Papathanasiou, S.; Psarras, S.; Mavroidis, M.; Capetanaki, Y. Strategies to Study Desmin in Cardiac Muscle and Culture Systems. *Methods Enzymol.* **2016**, *568*, 427−459.
(40) Weintraub, H. The Myod Family and Myogenesis: Redundancy, Networks, and Thresholds. *Cell* **1993**, *75*, 1241−1244.
(41) Solanki, A.; Shah, S.; Yin, P. T.; Lee, K.-B. Nanotopography-Mediated Reverse Uptake for Sirna Delivery into Neural Stem Cells to Enhance Neuronal Differentiation. *Sci. Rep.* **2013**, *3*, 1553.
(42) Langenbach, F.; Handschel, J. Effects of Dexamethasone, Ascorbic Acid and B-Glycerophosphate on the Osteogenic Differentiation of Stem Cells in Vitro. *Stem Cell Res. Ther.* **2013**, *4*, 1−7.
(43) Faia-Torres, A. B.; Goren, T.; Ihalainen, T. O.; Guimond-Lischer, S.; Charnley, M.; Rottmar, M.; Maniura-Weber, K.; Spencer, N. D.; Reis, R. L.; Textor, M.; Neves, N. M. Regulation of Human Mesenchymal Stem Cell Osteogenesis by Specific Surface Density of Fibronectin: A Gradient Study. *ACS Appl. Mater. Interfaces* **2015**, *7*, 2367−2375.
(44) Rosen, V. Bmp2 Signaling in Bone Development and Repair. *Cytokine Growth Factor Rev.* **2009**, *20*, 475−480.
(45) Bittner, S. M.; Guo, J. L.; Mikos, A. G. Spatiotemporal Control of Growth Factors in Three-Dimensional Printed Scaffolds. *Bioprinting* **2018**, *12*, No. e00032.
(46) Dang, M.; Saunders, L.; Niu, X.; Fan, Y.; Ma, P. X. Biomimetic Delivery of Signals for Bone Tissue Engineering. *Bone Res.* **2018**, *6*, 1−12.

https://doi.org/10.1021/acsami.2c10288
ACS Appl. Mater. Interfaces 2022, 14, 34488−34501

(47) Xiao, P.; Qiu, N.; Gu, J.; Wang, S.; He, J.; Huang, C.-F.; Zhang, J.; Huang, Y.; Chen, T. Direct Supramolecular Interacted Graphene Oxide Assembly on Graphene as an Active and Defect-Free Functional Platform. *Chem. Commun.* **2017**, *53*, 1949−1952.
(48) Hirtz, M.; Oikonomou, A.; Georgiou, T.; Fuchs, H.; Vijayaraghavan, A. Multiplexed Biomimetic Lipid Membranes on Graphene by Dip-Pen Nanolithography. *Nat. Commun.* **2013**, *4*, 1−8.
(49) Zakrzewski, W.; Dobrzyński, M.; Szymonowicz, M.; Rybak, Z. Stem Cells: Past, Present, and Future. *Stem Cell Res. Ther.* **2019**, *10*, 1−22.
(50) Nezakati, T.; Cousins, B. G.; Seifalian, A. M. Toxicology of Chemically Modified Graphene-Based Materials for Medical Application. *Arch. Toxicol.* **2014**, *88*, 1987−2012.
(51) Mikami, Y.; Lee, M.; Irie, S.; Honda, M. J. Dexamethasone Modulates Osteogenesis and Adipogenesis with Regulation of Osterix Expression in Rat Calvaria-Derived Cells. *J. Cell. Physiol.* **2011**, *226*, 739−748.
(52) Shintani, N.; Hunziker, E. B.; Hunziker, E. Differential Effects of Dexamethasone on the Chondrogenesis of Mesenchymal Stromal Cells: Influence of Microenvironment, Tissue Origin and Growth Factor. *Eur. Cells Mater.* **2011**, *22*, 302−320.

https://doi.org/10.1021/acsami.2c10288
ACS Appl. Mater. Interfaces 2022, 14, 34488−34501